International Journal of Machine Tools & Manufacture 65 (2013) 29–36

Contents lists available at SciVerse ScienceDirect

International Journal of Machine Tools & Manufacture

journal homepage: www.elsevier.com/locate/ijmactool

An investigation of the mechanics of roller burnishing through finite element simulation and experiments

Pascale Balland [a,*], Laurent Tabourot [a], Fabien Degre [a], Vincent Moreau [b]

[a] Université de Savoie, laboratoire SYMME, BP 80439, 74 944 Annecy-le-Vieux Cedex, France
[b] Centre Technique du Décolletage, BP 65, 74301 Cluses Cedex, France

ARTICLE INFO

Article history:
Received 29 March 2012
Received in revised form
3 September 2012
Accepted 5 September 2012
Available online 17 September 2012

Keywords:
Roller burnishing
Deep rolling
3D finite element model

ABSTRACT

Roller burnishing is a surface treatment process that is of particular economic interest but not really well optimised. Due to a necessarily high degree of mesh refinement, until now the modelling of the process is rather limited to 2D plane strain finite element simulation. In order to account for fully tridimensional induced stress state, a 3D finite element model of the industrial burnishing process is proposed. A specific strategy consisting in determining a representative layer of the part and a minimum number of cycles is necessary to obtain results that can be compared to experimental ones. The quality of the obtained results in a reasonable simulation time demonstrates the possibility to efficiently use full 3D simulation for the burnishing process.

1. Introduction

Roller burnishing is an iterative mechanical process, mostly used on a lathe to induce superficial plastic strain to reduce the surface roughness of cylindrical machined parts with some advantages. This operation avoids costly supplementary grinding operations. Additionally, this finishing procedure has less impact on the environment than most other processes.

The roller burnishing principle is to use, instead of a cutting tool, a free roller that will sweep the whole cylindrical surface of the machined part. A force, whose direction is normal to the machined cylinder, is applied to the roller in order to generate high local stresses that will induce the plastic strain necessary to smooth surface irregularities. The governing parameters of the process are the geometry of the roller, the applied force, the relative tangential velocity between the roller and the part and the shift at each part revolution. Good combination of these parameters leads to roughness decrease and beneficial compressive stress for part submitted to fatigue during service [1]. Meanwhile, the surface hardness is increased through the subsequent hardening of the material due to the plastic strain [2].

This process is not widely studied in the literature but has already been the subject of few experimental and numerical studies. Black and al. [3] interpreted experimental results with an analytical model based on strong schematisation of the burnishing. The works of Hassan et al. [4], El-Axir et al. [5], Luca et al. [6], El-Tayeb et al. [7,8] and Lopez de Lacalle et al. [9] are also noteworthy examples of all efforts made to connect process parameters and their effects on the machined part. However, the validity of these strongly experimentally-based models is limited to their specific associated experimental configurations and cannot be extrapolated in any way to other materials or situations. Indeed, due to the very heterogeneous strain field induced by the process, the only solution to obtain more generic and reliable models is to make use of finite element code to describe the process.

Finite element (FE) simulation of the strain field induced by indentation of a spherical rigid body in a metallic material was at the very beginning proposed by [10]. A more global 2D FE model of the process was proposed by [11] and concerns ball burnishing of a 100Cr6V sample that was previously tempered and machine finished. The size of the problem is reduced by observation of cylinders that have been ball burnished. After the process execution, the strains resulting from the process are only radial and tangential (see Fig. 1).

For the authors, this plane strain state is developed even during the application of the process and consequently 2D finite element modelling of the iterative forming phase itself should provide results consistent with experimental evidence. The effects of several shifted passages of the roller on the cylinder are thus supposed to be reproduced by several shifted indentations along the z of a planar rectangular shape by a circular tool following the y direction (y- and z-direction are given in Fig. 1). The roller is pressed against the part until the applied force along the z is equal to the experimentally measured applied force on the tool. Nevertheless, this model underestimates the penetration depth of the

* Corresponding author. Tel.: +33 450 096 566; fax: +33 450 096 543.
E-mail addresses: pascale.balland@univ-savoie.fr (P. Balland), laurent.tabourot@univ-savoie.fr (L. Tabourot), v.moreau@ctdec.com (V. Moreau).

0890-6955/$ - see front matter © 2012 Elsevier Ltd. All rights reserved.
http://dx.doi.org/10.1016/j.ijmachtools.2012.09.002

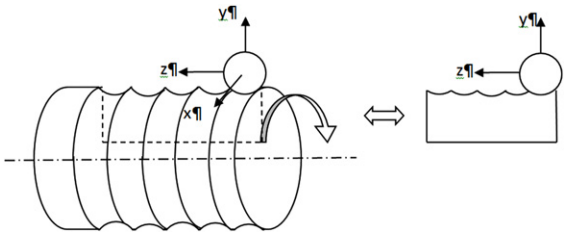

Fig. 1. Schematic transition from 3D to 2D representations of ball burnishing process.

rolling element. According to the author, this error is due to the line contact induced by the plain strain assumption.

To obtain more consistent results, Yen et al. [12] impose displacement of the ball. The penetration depth of the roller is therefore estimated by a three-dimensional simulation of the single path of the rolling ball on a parallelepiped, which represents the surface layer of the part. More recently Sartkulvanich et al. [13] have improved this 2D model by determining the flow stress of the work piece surface using instrumented ball indentation tests in conjunction with FE inverse analysis. The burnishing force is calibrated by considering pressure loss during FE simulations and initial surface roughness and residual stresses determined from hard turning experiments are introduced in the numerical model. Results have been validated with hard roller burnishing experiments.

Despite of all these improvements, several factors are pointed out by the authors as sources of discrepancies between the simulation and the experimental results. Indeed, 2D modelling remains a stopgap due to high simulation cost regarding full 3D modelling. Therefore, the main origin of gaps is that plane stress hypothesis cannot be applied during the dynamic stage of burnishing that leads to the forming of the furrow and the ridge in front of the ball. In [14], the ridge phenomenon that affects the mechanics of the process is demonstrated, allowing for improved modelling of the burnishing process

Experimental evidence of these fully 3D mechanisms are to be found in [15] where experimental evidence of a frontal ridge pushed by the ball is given. It is therefore very clear that this ridge formation and its subsequent complex strain history cannot be taken into account by only 2D indentations. The price to pay for better results is to develop 3D FE modelling; the increase in computing time is only a technical point that one can expect to be quickly solved in the future. Nowadays computers have gained in powerfulness and allow some new attempts in this direction.

Therefore, this paper presents a 3D FE model applied to a real industrial case of roller burnishing in which the model volume is reduced by considering only a portion of the surface layer of the piece. The accuracy of the model is evaluated regarding the results of an experiment where the roughness, the surface hardness and the distribution of residual stresses are evaluated. The developments of this paper take place in a context of SMEs and their affiliated technical centre which imposes strong attention to the quality of the results vs. cost ratio. The plan of this paper runs as follows.

In a first section, the experimental data are presented. In a second one, the finite element modelling is presented. Comparison between simulated results and the experimental results are the matter of the third section. Finally, conclusions and perspectives of this study are drawn.

2. Experimental procedure

The material used in this study is an alloyed steel whose industrial designation is 11SMn30 delivered in the form of bars. The original diameter of the bar is 30 mm. It is machined with an industrial lathe (DMG Sprint 32) with a carbide cutting tool (0.8 mm radius). Final machined diameter is 28 mm. The machining characteristics are: feed rate=0.15 mm/turn and cutting speed=200 m/min.

Table 1
Characteristics of the simulated experiment.

Piece diameter	Roughness period	Roughness height	Burnishing radial force	Burnishing speed	Burnishing feed rate
28 mm	0.15 mm	6.6 μm	230 N	100 m/min	0.15 mm tr^{-1}

Table 2
Effects of burnishing.

Machined roughness (R_z)	Machined roughness period (R_{sm})	Raw material hardness	Burnished roughness (R_z)	Burnished roughness period (R_{sm})	Burnished surface roughness
6.6 μm	0.15 mm	175 Hv0.1	1.2 μm	0.1 mm	264 HV0.1

The burnishing tool employed is an Ecoroll EG-5 which is a single roller tool. The roller is made of steel and his axis makes a 1.5° angle with the workpiece axis. The hardness of the roller is not provided by the manufacturer.

The lathe is equipped with a Kistler measurement system. This three component dynamometer (reference 9257BA) provides force values along the axial, tangential and radial directions during the burnishing operation. The trajectory of the burnishing tool consists in three steps. First, while the workpiece is turning, the roller is pressed against until 50% of the nominal force is reached. Then, the tool is subjected to a combined trajectory: the tool is moved radially in order to reach the nominal force while it covers 4 mm in the axial direction. Finally, the radial coordinates are fixed and the roller burnishes the part with a rectilinear trajectory. Lubrication is employed during all the experiment. As only the half of the part is burnished, the final part shows a machined zone and a burnished zone. The characteristics of the burnishing operation are listed in Table 1. Effects of burnishing are summarised in Table 2.

3. FE modelling of the roller burnishing process

The leading idea to build a finite element model is to find a configuration that is sufficiently representative to give back phenomena that occur during the modelled process. This simple idea is often annoyed, like in the present case of ball burnishing, by the required size of the simulation. Burnishing induces very strong strain gradients occurring on very small layer and requires very fine mesh. Therefore one is obliged to find a reasonable strategy to obtain with a given model pertinent results in acceptable simulation time. The complex kinematical conditions applied to the roller and the part are well described with connectors provided in Abaqus FE software which is used in the present study.

This section is devoted to the presentation of the finite element modelling of ball burnishing. First, the material characterisation and modelling is presented. The second part is devoted to the design of the geometric model including meshing. The boundary limit conditions are described in the third part.

3.1. Material characterisation and modelling

The objective of the identification is to provide robust modelling of the material. Elastic properties as well as plastic properties

should be identified. The goal of this paper being to show 3D FE simulation feasibility, efficient procedure has been privileged in this field. Indeed, the material modelling could have been very sophisticated due to the heterogeneities that are usually observable at different level of ball burnished material. These heterogeneities are generated by the elaboration process of the bar and after by machining that induces strong structure changes in a thin surface layer. Strain path applied by the roller is also very complex. The possibilities for material modelling are wide and could include the material heterogeneity, the complex path and cyclic effect imposed by the roller, strain rate sensibility… In this situation, it is not usually proven that complex modelling will provide real improvement on the quality of results, therefore only a few aspects that are considered as essential for this study are retained. The material is considered to be isotropic, not sensible to strain rate in the range of those imposed by the process and mean behaviour is considered due to impact of the roller on the material larger than the affected zone by machining. As roller imposes mainly large compressive strains on the material, the choice of a global compressive test has been made to carry out the identification of the plastic model.

Elastic characteristics of the material were identified with an ultrasonic device (Olympus 38DL Plus ultrasonic thickness gage).

The measurement principle is based on the dependence between the elastic modulus E, the Poisson's ratio v, the density ρ and the propagation speed of transverse C_T and longitudinal C_L ultrasonic waves according to the two following relations:

$$v = \frac{1-2(C_T/C_L)^2}{2-2(C_T/C_L)^2} \quad (1)$$

$$E = 2\rho C_L^2(1+v) \quad (2)$$

Contact transducers, which simultaneously act as emitter and receptor, were used. The frequencies were 10 MHz for longitudinal waves and 5 MHz for transverse waves. Three parallelepipeds (10 mm × 10 mm × 15 mm) specimens were cut at the centre of the bar. The results, synthetically represented in Table 3, produced the following average values: $E=198$ GPa and $v=0.3$.

Preliminary tests have been carried out in order to define main options to adequately describe plastic behaviour of the material. The material fit to the category of elasto-plastic material with isotropic hardening. This model is available in the library module of Abaqus. The corresponding stress–strain reference curve is determined with a compression test, which is more suitable, regarding the large compressive strains applied by the roller burnishing process, than classical tensile test. One another advantage is that this test can be easily used in SMEs that have not large equipment to their disposal. Indeed, the tensile test, whatever the device is (tensile machine, split Hopkinson bar test) provides stress–strain curves that covers too much limited strain range due to occurrence of necking. Complementary methods, such as the Bridgman method [16], enable the use of data obtained after the necking appears but it is still not sufficient to reach the strain imposed during ball burnishing (FE computations show an equivalent plastic strain of 150%)

Therefore, in order to observe the material behaviour at large strains, compression tests were developed. A "Rastegaev"-type geometry [17] (see Fig. 2) was used in order to limit the friction phenomena that occur at the sample-plate interface. Testing was conducted on a 600 kN electro-mechanical traction-compression machine. The deformation of the sample was determined from the displacement sensor of the machine. Because this sensor is located at some distance from the sample, the displacement data was corrected to take into account of the stiffness of the machine by subtracting a stiffness curve obtained using raw data collected pressing grip against grip. The dimensions of the 3 tested samples which were established in accordance with Pöhlandt's recommendations [18] are listed in Table 4. The stress was applied using a displacement speed of 1 mm min^{-1}. Fig. 3 presents the reference Cauchy stress versus plastic strain curve that is introduced as a classical metal plasticity model.

Table 3
Elasticity coefficients of the studied material measured by ultrasonic method.

	Sample 1	Sample 2	Sample 3
E (GPa)	200	197	197
v	0.29	0.30	0.30

3.2. Geometry and meshing

The definition of the size of the studied geometry and its associated meshing is the most critical of all because the idea is to make significant progress in this field, by moving from 2D modelling to 3D modelling. The choice of the representative

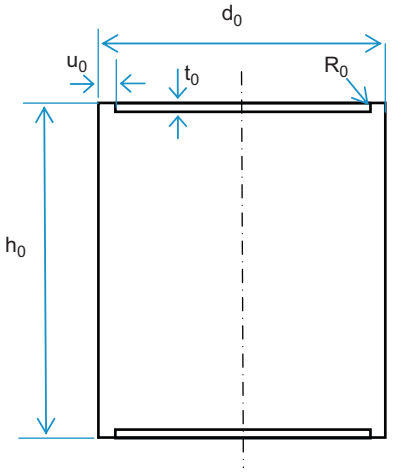

Fig. 2. Schematic representation of a Rastegaev-type sample.

Table 4
Dimensions of the Rastegaev-type compression sample.

	h_0	d_0	u_0	t_0	R_0
Dimensions (mm)	20	20	1	0.4	0.2 max

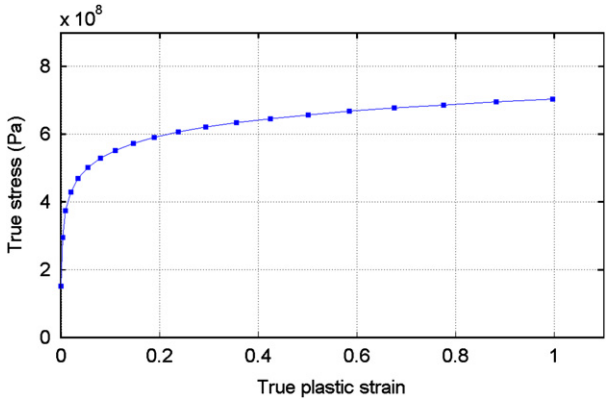

Fig. 3. Hardening curve obtained from compression test on the studied material.

volume is therefore of primary importance. As the process applies the same deformation everywhere on the surface layer, it is clear that it is not necessary to model the entire part. Furthermore, as it affects only a layer whose thickness is small regarding to the diameter of the part, only a small superficial layer of the part has to be considered.

Ball burnishing imposes strong strain gradient which requires very fine mesh near the surface along the direction *y*. Furthermore, the description of roughness (typical distance between peak: 0.15 mm) requires several elements. When going to the core, mesh can be coarse because material remains unaffected. Provided that the piece dimensions are large compared to the dimensions of the zone of contact, the pressures in the piece are independent of its overall geometry [19] and are thus estimated without considering the "far" region(s) neighbouring the zone of contact. During this process, the entire surface of the piece comes into contact with the roller. However, because this contact occurs in an identical way at any time, it is possible to represent the entire process using only a portion of the piece. Fig. 4 depicts the location of this volume in the piece. The non-representative portion of the piece can be modelled as a volume with semi-infinite elements. The dimensions of the representative volume (3.75 mm in the axial direction, 2.5 mm in the radial direction and 15° in the circumferential direction) of the piece are the smallest ones that keep the solution unchanged regarding the full problem.

The influence of the orientation of the machining striations (or of the helical angle of the striations) is presumed to be negligible. As a consequence, the surface of the representative portion of the piece is constructed by the revolution (around the axis of the piece) of a profile of roughness. The dimensions of the profile are adapted to the effective roughness of the rough shape. The real form of the roughness profile is modelled by a periodic triangular profile.

The representative portion of the piece is discretised in solid hexahedral 3D elements with linear interpolation and reduced integration. These elements provide displacement for each of the eight nodes and pressure for the one point of integration. The unconsidered portion of the piece is modelled using hexahedral, semi-infinite elements with linear shapes. These elements have eight nodes. The four first nodes are common to the finite elements constituting the boundary. The four other nodes are defined by a central symmetry relative to a reference point, called a pole. The roller is considered as rigid and is modelled by an analytical surface.

The representative portion of the piece is segmented into three independent parts. The surface grid is generated by rotating around the *z* axis of a 2D mesh described initially in the (rOz) plane. The three parts are connected via displacement constraints. Accordingly, the master surface transmits the movements of each of the concerned nodes to the slave surface. The used meshing is represented in Fig. 5. The model requires 92 292 hexahedral C3D8R elements of order one and 3 102 CIN3D8 semi-infinite elements of order one.

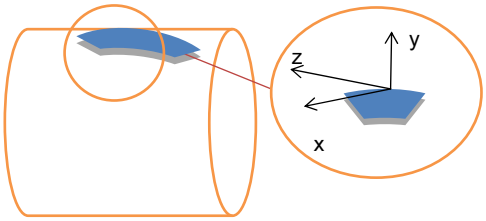

Fig. 4. Schematic representation of the representative portion of the workpiece. Dimensions of the representative volume are 3.75 mm in the axial direction *z*, 2.5 mm in the radial direction *r* and 15° around the axis *z*.

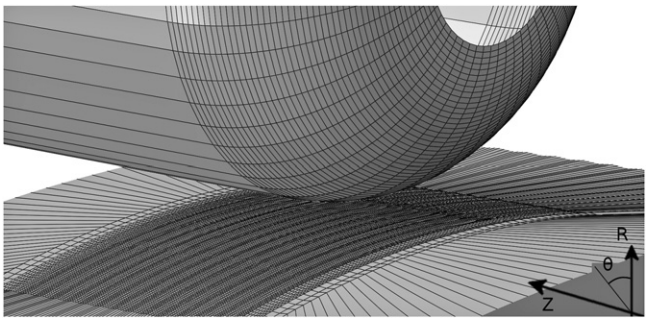

Fig. 5. Meshing for 3D roller burnishing model (dimensions are 3.75 mm in the axial direction, 2.5 mm in the radial direction and 15° in the circumferential direction).

3.3. Boundary conditions

To optimise the calculation times, the initial kinematics of roller burnishing which is a translation of a tool combined to the rotation of the part is reversed into a turning, tool relatively to a fixed piece. In this way, the costly stages of node projections at each time interval are avoided. The contact inducted by the roller burnishing process exhibits an evolutionary character from turn to turn. Thus, many turns of the piece are necessary to obtain an established regime. The kinematics of the roller burnishing model is thus constituted by a minimum number of cycles, each of them corresponding to a revolution of the piece. Each cycle is composed of six stages.

The initiation of contact between the piece and the roller occurs during the preload stage. The movement of the roller is driven by force. To avoid the contact detection problems induced by the quasi-static resolution method, a viscous damping is introduced between contact pair (ABAQUS/Standard STABILISE option). This bulk viscosity is purely artificial and is used to dampen inertia effect. Additionally, to ensure that this initial procedure does not affect the final displacement of the roller, this viscosity coefficient is diminished during this stage to reach a final value of zero. Next, an indentation stage is initiated. The burnishing force is applied to the roller until it approaches its equilibrium position thereby limiting the angular portion necessary for reaching stabilisation. Next the roller burnishing stage comes, during which the roller undergoes a pseudo-circular trajectory on a given angular portion. At the end of this stage, the roller is moved upwards in order to allow the elastic return of the material. Subsequently, the roller is displaced a few micrometres above the surface to avoid interaction during the return stage. Finally, the last stage consists of bringing the roller back to its initial angular position while applying an axial translation equal to the axial displacement of the tool after one revolution of the part.

The boundary conditions are transmitted to the roller via connectors. These elements, specific to the software ABAQUS and behaving as mechanical connections, enable to define connections between two master points (for example pivot or translation). Therefore, each connector possesses its own degrees of freedom, and the kinematics conditions can be applied according to the non-constrained directions. In the present case, two connectors are used. A schematic representation is presented in Fig. 6. The connectors are represented by large dotted lines, and their degrees of freedom are designated with arrows. Connector C1 which connects point A (located on the axis of the piece) to point B (located on the axis of the roller) allows a translation. Connector C2 which links point B to the reference point of roller C (also located on the roller axis and piloting the movements of the roller) allows a rotation. In this way, the pseudo-circular

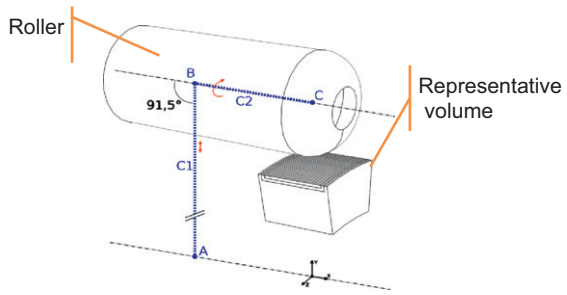

Fig. 6. Schematic representation of the connectors used to impose the boundary conditions on the roller. The dimensions of the representative volume are 3.75 mm in the axial direction, 2.5 mm in the radial direction and 15° in the circumferential direction.

Table 5
Boundary conditions of the roller burnishing model for one cycle.

	Point A: U_x	Point A: UR_x	C1: U	C1: F	C2: UR
Pre-load	0	0	Ø	$0.1F$	0
Indentation	0	0	Ø	F	0
Roller burnishing	0	Γ	Ø	F	0 if $\mu=0$, Ø if not
Elastic return	0	0	Ø	Ø	0 if $\mu=0$, Ø if not
Recovery	0	0	$3R_z$	Ø	0
Return	V_f	$-\gamma$	0	Ø	0

trajectory of the roller around the piece is piloted by the rotation around the axis (Ax). The force of the burnishing, which is normal to the surface of the piece, is imposed on the roller via a boundary force condition on connector C1. The degree of freedom of connector C2 allows the free rotation of the roller on its own axis when friction is introduced between the piece and the tool. Finally, the shift of the roller in the x direction, which corresponds to the tool displacement for each turn of the piece, is piloted via the displacement of point A. The boundary conditions of point A, the degree of freedom of connector C1 and the degree of freedom of connector C2 for each of the 6 stages of the cycle are summarised in Table 5.

V_f is the pace of advancement of the tool, γ is the angular portion necessary for the stabilisation of the rolling contact, R_z is the height of the roughness of the piece, F is the force of the burnishing, μ is the friction coefficient, and Ø specifies a non-constrained degree of freedom.

With regard to modelling the contact, the contact is managed by the means of a rigid, master-slave contact algorithm. The friction is taken into account using a penalty method and a value of 0.2 for μ.

Initiation of the roller burnishing process involves setting the motions of the piece and the tool. In this study, we chose not to consider the transitory accelerating phases in order to focus on the process in the established regime represented here by a succession of steps in which the static equilibrium is respected. Because the dynamic effects and the viscous behaviour of the material have not been considered, the velocity of the roller does not affect the solution. In addition, each stage of the contact cycle is established in an identical time interval that is equal to 1 s. In the case of quasi-static analyses, Abaqus offers only one possibility relating to the resolution algorithm. Thus, this implicit integration schema is based on a Newtonian resolution method.

The characteristics of the simulation are described in Table 5. Twelve cycles of contact, corresponding to twelve piece revolutions, are necessary to achieve a steady state. For this simulation, the dimensions are 3.75 mm in the axial direction, 2.5 mm in the radial direction and 15° in the circumferential direction. A burnishing force F is applied to the roller, and under this load, the roller moves an angular portion of $\gamma=8°$ corresponding to a peripheral distance of 2 mm. Such a displacement is necessary for the stabilisation of the rolling contact. Calculation takes about 7 days and needs 6 Go of RAM.

4. Results and discussion

At the end of the 12 simulation cycles, the surface profile is generated along the line of the cylinder. Gaussian filtering is executed with a 0.8 mm cut-off frequency to distinguish between the waviness and roughness components. Fig. 7 presents the various profiles.

The evolution of the primary profile reveals the influence of the transitory regime (that occurs during the first turns of the piece) on the geometry of the surface. During the first simulation cycles, the roller tends to increase its penetration (into the piece) with each cycle, thereby inducing a descending profile. This phenomenon can be explained by the fact that the roller progressively moves out of the furrow formed during the first cycle. The contact surface then tends to diminish in the axial direction, generating even deeper roller penetration. Thus, matter tends to accumulate with each cycle. As a result, the contact surface between the roller and the piece tends to increase (in this direction), thereby reducing the penetrating depth of the roller which explains the ascending evolution of the primary profile in the axial coordinate interval $[0.6e^{-3};1.6e^{-3}]$ m. During subsequent cycles, the penetrating depth of the roller becomes stable, and the solicitation enters in an established regime. The amplitude of the lateral projection is clearly visible in the coordinate interval $[2.1e^{-3}; 2.5e^{-3}]$ m in the profiles of Fig. 7. Consequently, the evolution of the stress in the transitory state induces variation in the residual height of the roughness (inset graph of Fig. 7). Thus, during the first paths of the tools, the deep penetration of the roller substantially smoothers out the irregularities of the surface. Then, with greater number of paths, the amplitudes of the irregularities vary until they reach a stable height.

The evolution of the height of the surface irregularities along the roughness profile is presented in Fig. 8. The amplitudes of the roughness peaks appear to vary in the first part of the profile and are thus deformed in the transitory regime. The height of the surface roughness subsequently converges to a stable value, at which point having reached the deformed zone in the steady state. This stable value thus constitutes the main characteristic of the state of the burnished surface. It is worth noting that $R_z=1.3$ μm. Similarly, experiments conducted in an identical configuration gave a R_z of 1.2 μm (roughness height after burnishing) corresponding to a relative error of approximately 8%.

Finally, the distributions of residual pressures were extracted and compared to the experimental values obtained by X-ray diffraction. Fig. 9 presents a model/experiment comparison of the residual pressures relative to the maximum pressure in the axial direction. The experimental data were normalised by the maximum pressure measured in the axial direction. Similarly, the simulated data are normalised by the maximal value of the axial pressure profile generated by the simulation. In this case, a strong correlation is observed in the depth range $[0; 0.3e^{-3}]$ m. Beyond this depth, the experimental and simulated data diverge. This divergence can be attributed to the use inside the simulation of an insufficient depth (of the portion of the piece). According to Guo and Barkey [20] who studied the residual stress profile on rolling contact of hard machined components, this difference may be attributed to measurement errors and the numerical errors since the points are very close to the surface, which is beyond the capability of the employed test methods.

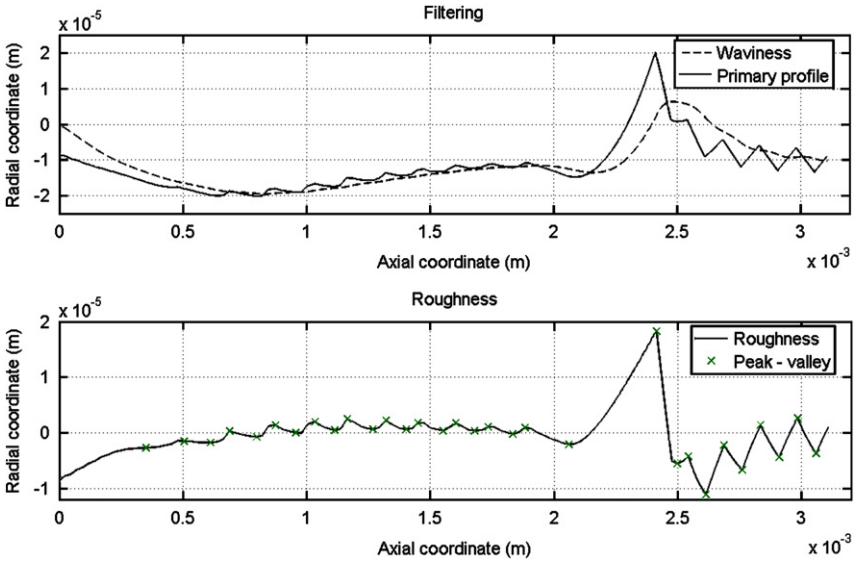

Fig. 7. Analysis of the roughness and waviness profiles of a burnished piece (simulation).

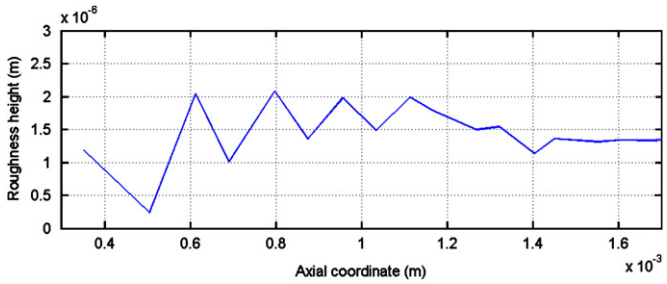

Fig. 8. Evolution of the heights of irregularities along the roughness profile (simulation).

In addition, the superficial micro-hardness of the digital piece was computed by simulations that employed a 3D model of the hardness testing. The mechanical characteristics measured at the end of the burnishing simulation (distribution of residual pressures and metalworking distribution which depend on the depth of the piece) were subsequently used as the initial conditions for the hardness testing model. Next, the hardness was calculated as the ratio between the applied effort and the contact surface under load. The precision of this model was qualified by comparing the simulated and experimental hardness values of the raw material. In this case, a 5% error was obtained.

Simulation of the hardness testing (on the burnished material) gives a contact surface (under load) of $4.71e^{-4}\,mm^2$, which corresponds to a micro-Vickers hardness of 212 HV0.1. Comparison with the value numerically obtained for the unused material indicates that burnishing results in a 46 HV0.1 gain in superficial hardness. However, experimental measurements on the surface of a burnished piece under similar conditions show a 264 HV0.1 surface hardness (with a standard deviation of 26 HV0.1), resulting in a discrepancy of 24% between the model and the physical experiment.

Studies of the machined surface reveal at least one clue regarding this discrepancy. At the end of the machining operation, a series of micro-hardness measurements were conducted on the piece under study. The average hardness was 236 HV0.1, and the standard deviation was 19 HV0.1. Thus, it appears that the machining operation has substantially modified the superficial hardness of the piece, with the raw material beginning with a hardness of 175 HV0.1 and the machined piece having a hardness of 236 HV0.1. On its left-hand side, Fig. 10 shows a micrograph which is based on a (rOz) cylindrical landmark of the surface of the machined piece. Two roughness peaks can be seen on the surface. A zone of a depth of several micrometres appears directly under the surface at the level of the roughness peaks. In this layer, the microstructure of the material appears disturbed. The line of the grains is not perceptible, and wavelets seem to indicate substantial material flow. This zone is extended to a roughly ten micrometres depth by the burnishing operation, as shown on the right-hand side of Fig. 10. This phenomenon was experimentally studied by Chou [21] on AISI 4340 steel (intermediary carbon rate) and the evolution of hardness was attributed to the hardening phenomenon, as well as a phase transformation.

Therefore, it appears difficult to predict the hardness of a burnished surface precisely without considering the mechanical modifications induced by the machining operation. Given the impact of residual pressures on the hardness test, one solution could be to experimentally determine the radial distribution of the hardening within the machined piece and to integrate it into the simulation of the burnishing operation. However, characterising this layer after it has been hardened is problematic. Indeed, micro-hardness measurements on a transversal section have not detected mechanical variations on/around the surface. This finding means that the thickness of the zone that has been hardened by machining is too small to be detected by using the hardness test on a transverse section. As a result, the digital prediction of the hardness of a burnished surface depends on the method used to characterise the mechanical state of the machined surface which is an entire new research direction. Understanding this phenomenon should assist in improving the reproducibility of burnished surface hardness measurements, thereby it should enable a better understanding of the effective gains resulting from the burnishing operation.

5. Conclusion

The burnishing process is an operation that is not industrially valued because of the difficulty in correlating the process parameters with geometrical and mechanical changes made to the part. However, this process is likely to provide significant added value that should not be neglected in the context of ever increasing competition. However, this valuation requires both

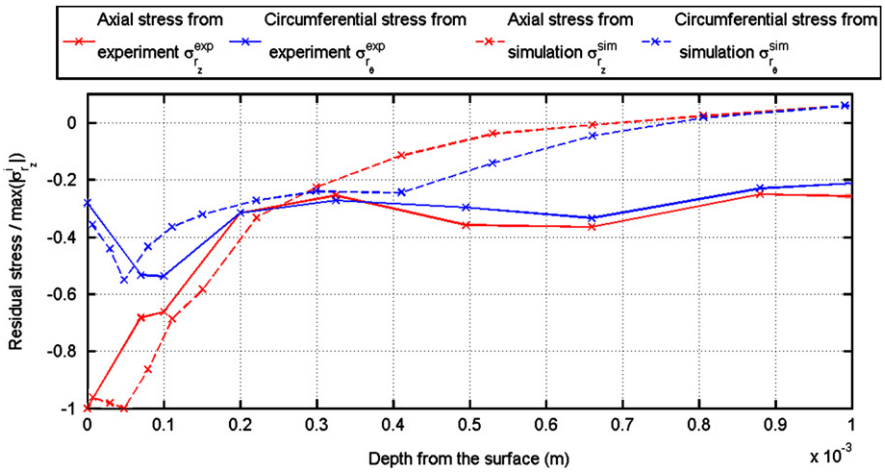

Fig. 9. Model-experiment comparison of the distributions of residual pressures. $\sigma^i_{r_z}$ refers to $\sigma^{exp}_{r_z}$ for experimental values and $\sigma^{sim}_{r_z}$ for simulated values.

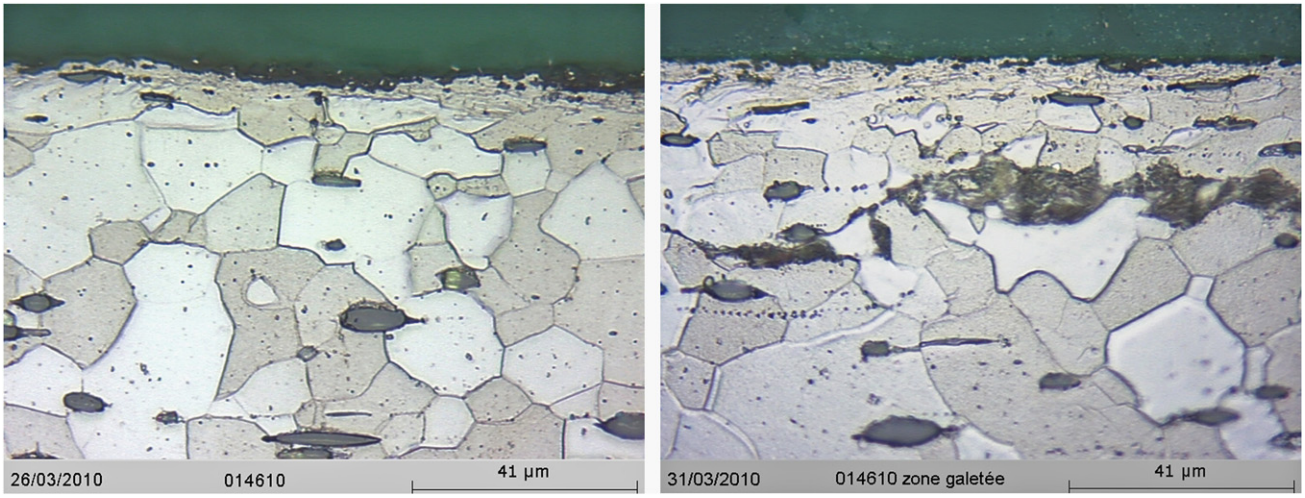

Fig. 10. Surface micrograph of a machined piece (on the left) and of a machined and subsequently burnished piece (on the right).

understanding the mechanisms of roller burnishing and controlling this process. That is why there has been a gradual development of numerical simulation of roller burnishing to one hand, to well understand its mechanisms and secondly to be able to optimise its different operations. Until recently, numerical studies were limited to 2D representations under plane strain assumptions. These hypotheses are too strong and impose artefacts to compensate plane strain effect that is finally not really applicable during the process. More realistic simulations are henceforth possible in 3D with the democratisation of computer grids. This paper promotes a 3D model simulation to study the process of roller burnishing. Measurements are made on a specific case of industrial ball burnishing of metallic part. The predictions of this model were comparable to experimental measurements. Concerning the geometric state of the surface, the numerical results well agree with the experimental measurements. Only a qualitative agreement is obtained with regard to mechanical values (surface hardness and residual pressure). Indeed, it is noted that mechanical behaviour is modified by the machining operation which induces structural evolutions. These results show that the effects of roller burnishing result from a complex interaction between the effects of roller burnishing and the machining that has proceeded. Machining induces a complex thermomechanical history that generates a distribution of mechanical properties on a very thin thickness not captured by any phenomenological model. The results show that the mechanical effect of roller burnishing is itself apprehensible through simulation. 3D simulation is indeed able to reproduce the effects of successive passages of the roller. In fact, it acts much like a plow which shapes the surface of the workpiece by pressing a ridge which will interact with the original profile of the part and the beads generated in the foregoing passages. Therefore, one understands that the parameters such as depth, pace of advancement are essential to control the roughness of the final part.

The use of simulation as a tool for process development, however, requires taking into account the heterogeneity of properties induced by machining. There are currently developments on models (compartmentalised models [22]) that can take them into account. This type of models, however, requires being able to determine the initial stress distribution into the simulation through detailed measurements of constraints, which is another experimental challenge.

Furthermore, in the light of these factors, one can understand that there is an additional option to optimise the effects of roller burnishing. It would be to cross the effects of machining and make roller burnishing get a part with even better features.

Acknowledgements

This study was conducted using funding from the Centre Technique de l'Industrie du Décolletage (CTDec). Calculations

were performed in the laboratory LAPP at the CNRS—Université de Savoie calculation meso-centre called MUST.

References

[1] R. Nalla, I. Altenberger, U. Noster, G. Liu, B. Scholtes, R. Ritchie, On the influence of mechanical surface treatments—deeprolling and laser shockpeening—on the fatigue behavior of Ti–6Al–4 V at ambient and elevated temperatures, Materials Science and Engineering: A 355 (2003) 216–230.
[2] N.H. Loh, S.C. Tam, S. Miyazawa, Statistical analyses of the effects of ballburnishingparameters on surface hardness, Wear 129 (1989) 235–243.
[3] A.J. Black, E.M. Kopalinsky, P.L.B. Oxley, Analysis and experimental investigation of a simplified burnishing process, International Journal of Mechanical Sciences 39 (1997) 629–635.
[4] A.M. Hassan, A.S. Al-Bsharat, Influence of burnishingprocess on surface roughness, hardness, and microstructure of some non-ferrousmetals, Wear 199 (1996) 1–8.
[5] M.H. El-Axir, An investigation into roller burnishing, International Journal of Machine Tools and Manufacture 40 (2000) 1603–1617.
[6] L. Luca, S. Neagu-Ventzel, I. Marinescu, Effects of working parameters on surface finish in ball-burnishing of hardened steels, Precision Engineering 29 (2005) 253–256.
[7] N.S.M. El-Tayeb, K.O. Low, P.V. Brevern, Influence of roller burnishing contact width and burnishing orientation on surface quality and tribologicalbehaviour of Aluminium 6061, Journal of Materials Processing Technology 186 (2007) 272–278.
[8] N.S.M. El-Tayeb, K.O. Low, P.V. Brevern, On the surface and tribologicalcharacteristics of burnishedcylindrical Al-6061, Tribology International 42 (2009) 320–326.
[9] L.N. López de Lacalle, A. Lamikiz, J.A. Sánchez, J.L. Arana, The effect of ballburnishing on heat-treatedsteel and Inconel 718 milled surfaces, International Journal of Advanced Manufacturing Technology 32 (2006) 958–968.
[10] K. Skalski, A. Morawski, W. Przybylski, Analysis of contact elastic-plastic strainsduring the process of burnishing, International Journal of Mechanical Sciences 37 (1995) 461–472.
[11] K. Roettger, Walzen hartgedrehter oberflaechen, PhD Thesis, WZL, RWTH Aachen, University, Aachen, Germany, 2002.
[12] Y.C. Yen, P. Sartkulvanich, T. Altan, Finite element modelling of roller burnishing process, CIRP Annals—Manufacturing Technology 54 (2005) 237–240.
[13] P. Sartkulvanich, T. Altan, F. Jasso, C. Rodriguez, Finite element modelling of hard roller burnishing: an analysis on the effects of process parameters upon surface finish and residual stresses, Journal of Manufacturing Science and Engineering 129 (2007) 705.
[14] P. Balland, L. Tabourot, F. Degré, V. Moreau, Mechanics of the burnishing process, Precision Engineering, http://dx.doi.org/10.1016/j.precisioneng.2012.07.008, in press.
[15] M. Barquins, M. Kennel, R. Courtel, Comportement de monocristaux de cuivre sous l'action de contact d'un frotteur hemispherique, Wear 11 (1968) 87–110.
[16] P. Bridgman, Studies in Large Plastic Flow and Fracture, With Special Emphasis on the Effects of Hydrostatic Pressure, Harvard University Press, Cambridge, 1964.
[17] M.V. Rastegaev, New Method of Homogeneous Upsetting of Specimens for the Determination of Flow Stress and the Coefficient of Internal Friction (in russian), 1940.
[18] W. Reiss, K. Pöhlandt, The Rastegaevupset test—a method to compress large material volumes homogeneously, Experimental Techniques 10 (1986) 20–24.
[19] K.L. Johnson, Contact Mechanics, Cambridge University Press, Cambridge, 1985.
[20] Y.B. Guo, M.E. Barkey, FE-simulation of the effects of machining-inducedresidual stress profile on rolling contact of hard machined components, International Journal of Mechanical Sciences 46 (2004) 371–388.
[21] Y.K. Chou, Surface hardening of AISI 4340 steel by machining: a preliminary investigation, Journal of Materials Processing Technology 124 (2002) 171–177.
[22] L. Tabourot, P. Balland, J. Raujol-Veillé, M. Vautrot, C. Déprés, F. Toussaint, Compartmentalised model for the mechanical behavior of titanium, Key Engineering Materials 504–506 (2012) 673–678.